SSRG International Journal of Civil Engineering
ISSN: 2348-8352/ https://doi.org/10.14445/23488352/IJCE-V13I9P115

Volume 13 Issue 9, 256-272, September 2026

Original Article

Remote Sensing-based Integration of Land Use/Land Cover, Vegetation Cover, and Land Surface Temperature with Hydrological Implications in Tikrit City, Iraq

Omar Taher Nafe'e[1], Dalia Shaker Mahdi[1], Lubna B. Mahmood[1] , Asmaa Abdul Jabbar Jamel[1*]

[1]*Tikrit University, College of Engineering, Salah Al-Din, Iraq.*

**Corresponding Author : ms.asmaajameel@tu.edu.iq*

Received: 15 July 2026 Revised: 24 August 2026 Accepted: 03 September 2026 Published: 29 September 2026

Abstract *- This study examines the integrated relationship among Land Use/Land Cover (LULC), Normalized Difference Vegetation Index (NDVI), and Land Surface Temperature (LST), with hydrological implications, in Tikrit City, Iraq, using Landsat data acquired in 2017 and 2025. LULC, NDVI, and LST layers were prepared using the same spatial boundary, and 4124 paired sample points were extracted from identical locations to support temporal and statistical comparison. The LULC results showed a clear reduction in Soil from 70.52% in 2017 to 49.88% in 2025, whereas Vegetation increased from 25.49% to 44.12%. Built Area also increased from 3.08% to 4.90%, indicating moderate urban expansion. The dominant land-cover transition was from Soil to Vegetation, covering 66,014.66 ha. Mean NDVI increased significantly from 0.061 to 0.075, while mean LST remained statistically stable, changing only from 41.992°C to 42.031°C. However, non-parametric tests indicated that the spatial distribution of LST changed significantly. The NDVI–LST relationship was positive in both years, with Pearson correlation increasing from 0.670 in 2017 to 0.709 in 2025. Regression analysis showed that NDVI explained 44.9% and 50.2% of LST variation in 2017 and 2025, respectively. Class-based analysis indicated that the dominant heat-contributing class shifted from Soil in 2017 to Built Area in 2025. These findings show that surface thermal behavior in Tikrit City cannot be explained by vegetation cover alone, but depends on land-cover composition, mixed pixels, agricultural activity, soil exposure, surface moisture, and seasonal conditions. From a hydrological perspective, the reduction of exposed soil, expansion of vegetation, and growth of built-up areas have implications for infiltration opportunity, runoff potential, evapotranspiration tendency, and surface moisture retention.*

Keywords *- Hydrological implications, Land Use/Land Cover, Vegetation index, Land surface temperature, Landsat, Remote sensing.*

1. Introduction

Land Use/Land Cover (LULC) change is one of the main indicators of physical transformation in urban and peri-urban environments. Changes in vegetation, bare soil, built-up surfaces, and water-related features affect surface reflectance, soil exposure, surface moisture, evapotranspiration tendency, infiltration opportunity, runoff potential, and Land Surface Temperature (LST).

In semi-arid cities, these processes are strongly linked because urban expansion, exposed dry soil, seasonal vegetation, and limited water surfaces can produce complex spatial patterns of vegetation response and surface heating.

Therefore, monitoring LULC change together with vegetation cover and LST is important for understanding surface thermal behavior and the potential hydrological implications of land-cover transformation.

Remote Sensing (RS) and Geographic Information System (GIS) techniques provide a practical framework for detecting these changes because they allow repeated, spatially consistent, and quantitative observation of the Earth's surface.

Landsat imagery is particularly useful for this purpose because it provides long-term multispectral and thermal records that can be used to classify LULC, calculate vegetation indices, retrieve LST, and compare surface conditions over time.

Previous studies in different regions, including watersheds, reservoirs, and urban areas, have confirmed the usefulness of RS and GIS for mapping vegetation, built-up areas, bare soil, and water bodies and for detecting temporal land-cover changes [1-3] In addition, reviews of Landsat time-series change detection emphasize the importance of consistent preprocessing and multi-temporal comparison before interpreting surface change [4].

In Iraq, RS- and GIS-based studies have increasingly been used to monitor land-cover dynamics in cities and agricultural regions. Studies conducted in Basra City, southern Iraq, and the Kufa–Najaf region showed measurable changes related to urban expansion, agricultural variation, bare-land transformation, and environmental pressure [5-7]. These studies provide useful evidence on the applicability of RS and GIS for LULC monitoring in Iraqi environments. However, most of them focused mainly on mapping land-cover classes and estimating area changes, with less attention to the combined interpretation of LULC change, vegetation response, surface temperature variation, and potential hydrological implications. This limitation is important in semi-arid Iraqi cities, where land-cover transformation may influence not only surface temperature but also infiltration opportunity, runoff tendency, moisture retention, and evapotranspiration potential.

The Normalized Difference Vegetation Index (NDVI) is widely used to represent vegetation condition because it depends on the contrast between red and near-infrared reflectance. This foundation is supported by early and widely used vegetation-index studies [8, 9], while recent reviews have emphasized the continued importance of NDVI in remote sensing applications [10]. Land Surface Temperature (LST), on the other hand, represents the thermal response of land surfaces and varies according to material properties, surface moisture, vegetation condition, bare soil exposure, and built-up intensity. Previous studies in Thailand and Imphal showed that the NDVI–LST relationship varies by location, season, land-cover type, and surface conditions [11, 12]. Although vegetation is commonly associated with lower LST through shading and evapotranspiration, the NDVI–LST relationship is not fixed. Positive NDVI–LST relationships may occur under mixed land-cover conditions, seasonal vegetation, agricultural surfaces, exposed soil–vegetation mixtures, or specific observation periods. Therefore, interpreting the NDVI–LST relationship requires considering LULC composition, mixed pixels, surface moisture, and seasonal conditions rather than assuming a uniform cooling effect of vegetation [13, 14].

The integration of LULC analysis, NDVI analysis, and LST analysis can give a more comprehensive understanding of surface dynamics than using each variable alone. LULC provides knowledge about the main type of cover on the surface, NDVI indicates the condition of vegetation, and LST indicates thermal properties of surface material. Previous urban and regional studies have shown that LST is influenced by built-up characteristics, spectral indicators, moisture conditions, and vegetation behavior. When these layers are analyzed together, they can reveal whether temperature patterns are controlled mainly by exposed soil, vegetation distribution, built-up expansion, surface moisture variation, or mixed pixels [15, 16]. Such integration can also support the interpretation of potential hydrological implications, because different land-cover classes differ in their likely effects on infiltration opportunity, runoff potential, evapotranspiration tendency, and surface moisture retention [17, 18].

Despite the growing use of RS and GIS in Iraq, limited work has examined Tikrit City using an integrated LULC–NDVI–LST framework supported by paired spatial sampling, transition analysis, classification accuracy assessment, and class-based statistical testing. In particular, there is still a need to determine whether vegetation change corresponds to thermal change at identical locations, whether LST differs significantly among LULC classes, and how land-cover transformation may indicate potential hydrological implications in a semi-arid Iraqi urban environment. This represents the main research gap addressed in the present study.

Accordingly, this study investigates the integrated relationship among LULC, NDVI, and LST in Tikrit City using Landsat data from 2017 and 2025. The study combines LULC classification and transition analysis, NDVI calculation, LST retrieval, paired spatial sampling, correlation and regression analysis, and class-based statistical testing. The novelty of this work lies in linking multi-temporal land-cover transformation with vegetation response, surface thermal behavior, and potential hydrological implications within a single statistical framework for Tikrit City. Unlike studies that focus only on LULC mapping or NDVI–LST correlation, this study evaluates spatial change, class transition, thermal redistribution, and land-cover-dependent NDVI–LST behavior together. The results are expected to support urban and environmental planning by identifying how land-cover changes may affect surface thermal patterns and potential surface-hydrological behavior in a semi-arid Iraqi city.

2. Study Area

Tikrit City, the administrative center of Salah Al-Din Governorate, is located in central-northern Iraq, approximately 180 km north of Baghdad. The study area extends approximately between 43°00′00″–44°00′00″ E longitude and 34°30′00″–35°00′00″ N latitude, as shown in Figure 1. According to the adopted spatial boundary, the selected area covers about 3,295.13 km². Tikrit represents an important urban area in Salah Al-Din Governorate and has experienced noticeable land-cover transformations during recent decades, mainly due to population growth, urban expansion, vegetation variation, and changes in open bare soil areas. These characteristics make the city a suitable case study for remote sensing-based monitoring of surface changes.

To assess Land Use/Land Cover (LULC) patterns, four dominant land-cover types were evaluated spatially: water, vegetation, built-up areas, and bare soil. The NDVI could also be used to assess vegetation density at different locations over your study area, while Land Surface Temperature (LST) may be used to evaluate the thermal characteristics of different surface materials.

More importantly, surface materials have strongly differing characteristics in terms of heat absorption and moisture availability, with built-up and bare ground having a greater potential for heat absorption and lower levels of moisture compared to vegetated surfaces and surfaces with water bodies, both of which reduce surface temperatures due to shading, moisture retention through surface infiltration, and evapotranspiration.

Because Tikrit has various urban land uses and surfaces (urban expansion, exposed soil, sporadically vegetated, and minimially water-covered), this region provides an ideal area to study differences in urban land use and surface types as they relate to the thermal distribution of the land surface. Therefore, Tikrit is a good place to conduct a study on how changes in land use and/or surface types affect land surface temperatures, and therefore to include land use/land cover, NDVI, and LST in the study of land cover variations and their spatial relationships to the land surface thermal patterns.

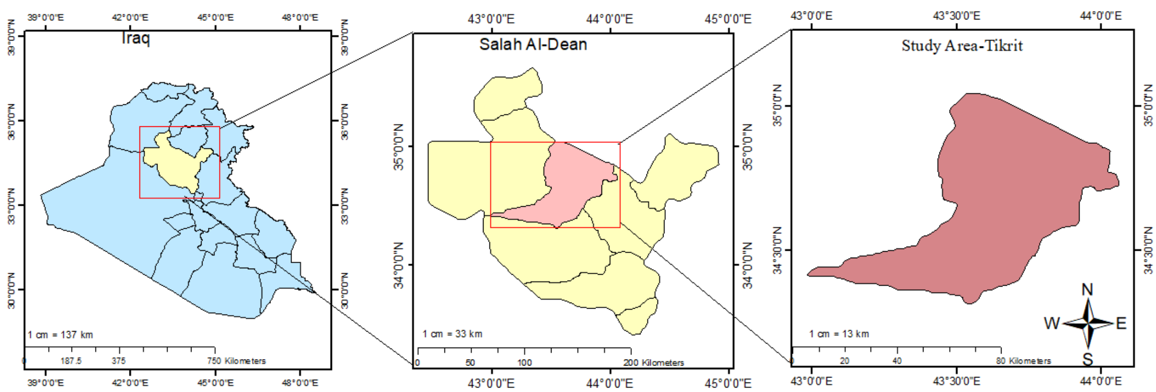

Fig. 1 Location map of the study area: (a) Iraq, (b) Salah Al-Din governorate, and (c) Tikrit City.

3. Materials and Methods

3.1. Satellite Data Source and Image Selection

Multi-temporal Landsat 8 Operational Land Imager/Thermal Infrared Sensor (OLI/TIRS) images were used to analyze Land Use/Land Cover (LULC), Normalized Difference Vegetation Index (NDVI), and Land Surface Temperature (LST) in Tikrit City. Two scenes acquired in March 2017 and March 2025 were selected from the United States Geological Survey (USGS) EarthExplorer platform. The use of images from the same month was adopted to reduce seasonal effects on vegetation cover and surface temperature, since both NDVI and LST are sensitive to seasonal variation. The selected scenes belonged to the same WRS path/row (169/36), which helped ensure spatial consistency between the two study years. Both scenes were obtained as Landsat Collection 2 Level-2 products to ensure consistency in sensor type, product level, acquisition season, and spatial reference.
Landsat Collection 2 Level-2 products offer substantial advantages in terms of providing atmospherically corrected Surface Reflectance (SR) bands and Surface Temperature (ST) data, thus achieving a higher level of consistency in vegetation and thermal analysis [19]. For LULC classification, the visible, near-infrared, and shortwave-infrared surface reflectance bands were used, including the blue, green, red, near-infrared, SWIR-1, and SWIR-2 bands. For NDVI calculation, the red and near-infrared bands were used, while the Level-2 surface temperature band ST_B10 was used for LST derivation. Additionally, the scenes were examined visually within Tikrit City, and no noticeable clouds or shadows were found to contaminate the region being studied. Several previous studies have used Landsat data to examine the integrated relationships among LULC, NDVI, and LST in urban and regional environments [14, 20].

All raster layers were projected and verified using the Universal Transverse Mercator (UTM) coordinate system, Zone 38N, based on the World Geodetic System 1984 (WGS 84) datum. The images were clipped to the same Tikrit City boundary to ensure that the 2017 and 2025 analyses were performed over an identical spatial extent. This step was necessary to allow direct overlay among the LULC, NDVI, and LST layers.

3.2. Image Pre-Processing

Before obtaining LULC, NDVI, and LST, all Landsat images were pre-processed in order to achieve spatial, radiometric, and temporal consistency. The pre-processing steps included visually inspecting the quality of the images, checking for obvious cloud or shadow contamination within the Tikrit City boundary, validating the image coordinates, and clipping the Landsat images to the defined geographic limits of Tikrit City. Pre-processing is important in multi-temporal remote sensing studies because geometric misalignment, cloud interference, and variable image area can produce errors in change detection and spatial comparisons [4].

For spectral analysis, surface reflectance bands were used because they reduce atmospheric effects and provide more reliable reflectance values for vegetation and land-cover analysis. The input feature set for LULC classification consisted of the visible, near-infrared, and shortwave-infrared surface reflectance bands. These bands were selected because they support spectral separation among water bodies, vegetation, built-up surfaces, and bare soil. For thermal analysis, the Landsat Collection 2 Level-2 surface temperature band was used to generate the LST layer. The use of Landsat Collection 2 Level-2 products is useful because these products provide atmospherically corrected surface reflectance and surface temperature layers, which improve consistency between the 2017 and 2025 datasets [19].

After pre-processing, all raster layers were aligned to the same projection, spatial resolution, and study boundary. This ensured that each pixel location represented the same ground area in all datasets. The resulting images served for supervised LULC classification, NDVI calculation and LST extraction, as well as for performing overlay analysis between land-use categories, vegetation and surface temperatures. This spatial alignment was also necessary for paired sampling, because NDVI and LST values from 2017 and 2025 were extracted from identical spatial locations.

3.3. Land Use/Land Cover Classification and Accuracy Assessment

The Land Use/Land Cover (LULC) maps for 2017 and 2025 were produced using a supervised classification approach. Four major LULC classes were identified based on the characteristics of the study area: water bodies, vegetation cover, built-up areas, and bare soil. These four classes were selected because they represent the dominant surface-cover types controlling the spectral, thermal, and potential hydrological behavior of the study area. Other minor or spectrally similar categories were not separated because of the 30 m spatial resolution of Landsat imagery and the possibility of spectral confusion among mixed urban, agricultural, and exposed-soil surfaces. Therefore, such surfaces were grouped into the most representative dominant class to reduce classification uncertainty and to maintain consistency between the 2017 and 2025 maps.

Training samples for each class were selected using visual interpretation of Landsat imagery and high-resolution reference images. The training samples were distributed across the study area to represent the spectral variability of each LULC class. Water samples were selected from river and water-covered areas, vegetation samples from cultivated and green areas, built-up samples from urban and impervious surfaces, and soil samples from bare or exposed land. The same classification scheme and class definitions were applied to both years to allow a reliable temporal comparison. The spectral signatures of the selected classes were then used to classify the Landsat images.

The Maximum Likelihood Classification (MLC) algorithm was applied because it is one of the most widely used supervised classification methods in remote sensing. The classifier assigns each pixel to the class with the highest probability of membership based on the statistical distribution of the training samples. Although recent studies have increasingly used machine-learning classifiers such as Random Forest, Support Vector Machine, and XGBoost, MLC was selected in this study because it is a well-established probabilistic classifier, performs effectively when representative training samples are available, and provides an interpretable statistical basis for multi-temporal Landsat classification. The objective of this study was not to compare classification algorithms, but to generate consistent LULC maps for integrating LULC, NDVI, and LST across two time periods. Therefore, MLC was considered appropriate for maintaining methodological consistency between 2017 and 2025. The general discriminant function used in maximum likelihood classification can be expressed as shown in Equation (1) [21, 22].

$$g_i(x) = lnP(\omega_i) - \frac{1}{2}\, ln \mid \Sigma_i \mid - \frac{1}{2}\,(x-\mu_i)^T\, \Sigma_i^{-1}\,(x-\mu_i) \quad (1)$$

Where $g_i(x)$is the discriminant function for class i, $x$is the spectral vector of the pixel, $P(\omega_i)$is the prior probability of class i, $\Sigma_i$is the covariance matrix, and $\mu_i$is the mean vector of class i. The pixel is assigned to the class that gives the highest value of $g_i(x)$. This method is suitable when representative training samples are available, and the spectral response of each class can be statistically described.

The classification accuracy was assessed using an error matrix, also known as a confusion matrix. A total of 200 stratified accuracy-assessment points were used for each year, with approximately 50 points distributed across each classified LULC class. Reference labels were assigned through visual interpretation of high-resolution satellite imagery and Landsat false-color composites. Points located on mixed or boundary pixels were assigned to the dominant visible surface-cover class. This rule was applied consistently to both years to reduce interpretation bias caused by mixed pixels and class-boundary uncertainty. The classified and reference labels were then compared using a confusion matrix. The main accuracy measures included Overall Accuracy (OA), Producer's Accuracy (PA), User's Accuracy (UA), and the Kappa coefficient (κ). These measures are commonly used to evaluate thematic land-cover classification accuracy [23, 24]. Overall accuracy was calculated using Equation (2):

$$OA = \frac{\sum_{i=1}^{r} n_{ii}}{N} \times 100 \quad (2)$$

Where OA is the overall accuracy, $n_{ii}$is the number of correctly classified samples for class i, $r$is the total number of classes, and $N$is the total number of reference samples.

Producer's accuracy and user's accuracy were calculated using Equation (3) and Equation (4), respectively:

$$PA_i = \frac{n_{ii}}{n_{+i}} \times 100 \quad (3)$$

$$UA_i = \frac{n_{ii}}{n_{i+}} \times 100 \quad (4)$$

where PA_i is the producer's accuracy for class i, UA_i is the user's accuracy for class i, n_{+i} is the column total for class i, and n_{i+} is the row total for class i, according to the adopted confusion matrix arrangement. Producer's accuracy indicates omission error, while user's accuracy indicates commission error.

The Kappa coefficient was calculated using Equation (5):

$$\kappa = \frac{(N \sum_{i=1}^{r} n_{ii} \ - \sum_{i=1}^{r} (n_{i+} n_{+i}) \ )}{\left(N^2 - \sum_{i=1}^{r} \ n_{i+} n_{+i} \ )\right)} \quad (5)$$

where κ is the Kappa coefficient, N is the total number of reference samples, n_{ii} is the number of correctly classified samples in class i, n_{i+} is the row total for class i, and n_{+i} is the column total for class i. The Kappa coefficient measures the agreement between the classified map and reference data after accounting for agreement that may occur by chance [24].

The resulting classified maps were then used to calculate the area percentage of each LULC class and to analyze spatial changes between 2017 and 2025. These classified layers also provided the basis for overlaying LULC with NDVI and LST in the subsequent analysis.

3.4. Normalized Difference Vegetation Index (NDVI) Calculation and Classification

The Normalized Difference Vegetation Index (NDVI) was calculated to evaluate vegetation cover and vegetation density within Tikrit City for 2017 and 2025. NDVI is one of the most widely used spectral vegetation indices in remote sensing because it depends on the contrast between red reflectance, which is strongly absorbed by vegetation chlorophyll, and near-infrared reflectance, which is strongly reflected by healthy vegetation [8, 9]. Consequently, the NDVI serves as a useful tool for differentiating vegetated areas from non-vegetated areas, and also to evaluate the spatial distribution of vegetation cover and density.

NDVI was selected in this study because it is simple, widely used, compatible with Landsat long-term datasets, and suitable for comparing vegetation response between different years. It also provides a direct and interpretable indicator for linking vegetation cover with LULC and LST patterns. However, the exclusive use of NDVI is acknowledged as a limitation, because other indices such as EVI, SAVI, MSAVI, and NDWI may provide additional information about vegetation structure, soil-background effects, and surface moisture conditions. These indices are recommended for future multi-index studies.

Concerning Landsat 8 OLI data, its near-infrared band comes under Band No. 5, whereas the red band comes under Band No. 4.[19]. Accordingly, NDVI was calculated using Equation (6):

$$NDVI = \frac{NIR - Red}{NIR + Red} \quad (6)$$

For Landsat 8–9 images, Equation (6) can be written in band form as Equation (7):

$$NDVI = \frac{Band\ 5 - Band\ 4}{Band\ 5 + Band\ 4} \quad (7)$$

where NIR is the near-infrared reflectance and Red is the red reflectance. The resulting NDVI values theoretically range from -1 to $+1$. Higher positive values indicate denser and healthier vegetation, while values close to zero or negative values generally represent bare soil, built-up areas, water bodies, or other non-vegetated surfaces.

To support quantitative comparison between 2017 and 2025, the NDVI raster was interpreted using predefined vegetation-cover ranges. These ranges were adapted from commonly used NDVI interpretation guidelines and adjusted to the observed NDVI range in the study area. The same NDVI ranges were applied to both years to ensure a consistent comparison. The adopted NDVI interpretation ranges are presented in Table 1.

Table 1. NDVI interpretation ranges used in the study

NDVI range	Interpretation
NDVI < 0.00	Water bodies or non-vegetated wet surfaces
0.00–0.10	Bare soil or very sparse vegetation
0.10–0.20	Low vegetation cover
0.20–0.40	Moderate vegetation cover
NDVI > 0.40	Relatively dense vegetation cover

The NDVI interpretation ranges were adapted from standard NDVI interpretation principles reported by USGS, NASA Earth Observatory, and USDA FAS. These ranges were used only for interpretation and visual comparison, not as a substitute for the original continuous NDVI values.

These categories were used only to support the interpretation of vegetation-cover conditions and their spatial relationship with LULC and LST. The original NDVI values were also retained as continuous variables for the statistical analysis, including descriptive statistics, correlation analysis, and regression analysis.

3.5. Land Surface Temperature (LST) Retrieval

The Land Surface Temperature (LST) was retrieved to evaluate the spatial thermal behavior of different surface-cover types in Tikrit City. In this study, LST was derived from the Landsat Collection 2 Level-2 Surface Temperature product rather than from manual radiance, brightness-temperature, and emissivity-correction steps. This approach was adopted because the Level-2 product provides a surface temperature band that has already been processed using the official USGS surface temperature algorithm [19, 25].

For the selected Landsat 8 scenes, the Level-2 surface temperature band $ST_{B10}$was used to generate the LST maps. The metadata files of the selected scenes indicated that the products were processed at Level-2 Science Product (L2SP) level and included the ST_{B10} surface temperature band.

The digital numbers of the ST_{B10} band were converted to surface temperature in Kelvin using the official scale factor and additive offset provided in the Landsat metadata file, as shown in Equation (9):

$$ST(K) = DN_{ST_{B10}} \times 0.00341802 + 149.0 \qquad (9)$$

where $ST(K)$ is the surface temperature in Kelvin, and is the digital number of the Landsat Level-2 surface temperature band.

The surface temperature in Kelvin was then converted to degrees Celsius using Equation (10):

$$LST(^{\circ}C = ST(K) - 273.15 \qquad (10)$$

Where $LST(^{\circ}C)$ is the land surface temperature in degrees Celsius. The resulting LST raster layers were clipped to the same Tikrit City boundary used for the LULC and NDVI layers to ensure spatial consistency among all datasets. LST was analyzed as a continuous temperature variable in degrees Celsius, while the color classes shown in the LST maps were used only for visualization. Therefore, no fixed LST threshold was used to define land-cover classes. The final LST maps for 2017 and 2025 were then used to compare the spatial distribution of surface temperature and to support the integrated analysis with LULC and NDVI.

3.6. Integration of Land Use/Land Cover, Vegetation Cover, and Land Surface Temperature

The integration of Land Use/Land Cover (LULC), Normalized Difference Vegetation Index (NDVI), and Land Surface Temperature (LST) was performed to examine how different surface-cover types and vegetation conditions were associated with the spatial distribution of surface temperature in Tikrit City. This integrated approach is useful because LULC classification identifies the dominant surface types, NDVI quantifies vegetation cover conditions, and LST represents the thermal response of the land surface. Similar studies have shown that combining LULC, NDVI, and LST provides a better interpretation of land surface thermal behavior than analyzing each variable separately [20].

The prepared LULC, NDVI, and LST raster layers for 2017 and 2025 were overlaid with the same spatial boundary, projection, and pixel resolution. This way, all the layers had the same footprint at each pixel location. LST statistics for each land-cover class (water bodies, vegetation cover, built-up areas, and bare soil) were extracted from the LULC maps. This step made possible the comparison of the thermal behaviour of different land cover classes.

Previous studies have reported that built-up and bare soil surfaces commonly show higher LST values, while vegetation and water-covered surfaces may show lower LST values due to shading, moisture availability, and evapotranspiration effects [14]. However, in the present study, these relationships were evaluated statistically rather than assumed in advance.

In addition, NDVI values were compared with LST values to assess the relationship between vegetation-cover conditions and surface temperature. High NDVI values generally represent denser vegetation, while low NDVI values may correspond to weak vegetation cover, bare soil, built-up surfaces, water bodies, or mixed surfaces. Thus, the comparison of NDVI with LST helps to find the observed thermal response related to vegetation conditions in the study area.

This wording is important because the NDVI–LST relationship may vary depending on land-cover composition, soil moisture, irrigation conditions, seasonal timing, and mixed-pixel effects. Previous research has confirmed that changes in vegetation cover and land-cover composition can significantly influence LST distribution, especially in urban and semi-urban regions [14].

Because Landsat pixels have a spatial resolution of 30 m, some pixels located along class boundaries or heterogeneous surfaces may contain more than one land-cover type. These mixed or boundary pixels were interpreted according to the dominant visible surface-cover class during visual interpretation and accuracy assessment. This procedure was applied consistently to both 2017 and 2025 to reduce interpretation bias.

LST was analyzed as a continuous temperature variable in degrees Celsius. The color classes shown in the LST maps were used only for visualization and map interpretation; therefore, no fixed LST threshold was used to define land-cover classes. This clarification was necessary because the LULC classes were derived from supervised classification, while LST was used to describe the thermal response of the surface.

To quantify the temporal changes between 2017 and 2025, the percentage change in each LULC or NDVI class was calculated using Equation (11):

$$Change\ (\%) = \frac{A_{2025} - A_{2017}}{A_{2017}} \times 100 \qquad (11)$$

where A_{2017} and A_{2025} represent the area of a specific class in 2017 and 2025, respectively. Positive values indicate an increase in class area, whereas negative values indicate a decrease. This equation was applied to evaluate the changes in LULC classes and NDVI vegetation categories during the study period.

The area percentage for each land-use class was computed based on the number of pixels belonging to a specific land-use class relative to the total number of valid pixels in the study area. This permitted the creation of comparative charts and tables for LULC, NDVI, and LST. The combined dataset was then used to correlate vegetation-cover variation, built-up areas, bare soil, and water bodies with surface temperature changes. The integrated analysis also supported the discussion of potential hydrological implications, including infiltration opportunity, runoff potential, surface moisture retention, and evapotranspiration tendency. However, these implications were interpreted indirectly from LULC, NDVI, and LST patterns. No direct hydrological measurements, runoff simulation, infiltration modeling, evapotranspiration estimation, or soil-moisture measurements were performed in this study. Therefore, the hydrological discussion should be understood as an interpretation of potential implications rather than measured hydrological outcomes.

4. Results and Discussion

4.1. Land Use/Land Cover Changes during 2017–2025

Figure 2 Land Use/Land Cover (LULC) maps of Tikrit City in 2017 and 2025. The LULC outputs were categorised into four main groups: Water, Vegetation, Built Area and Soil. These classes were used to quantify land cover distribution and temporal changes, and to facilitate the subsequent integration with NDVI and LST.

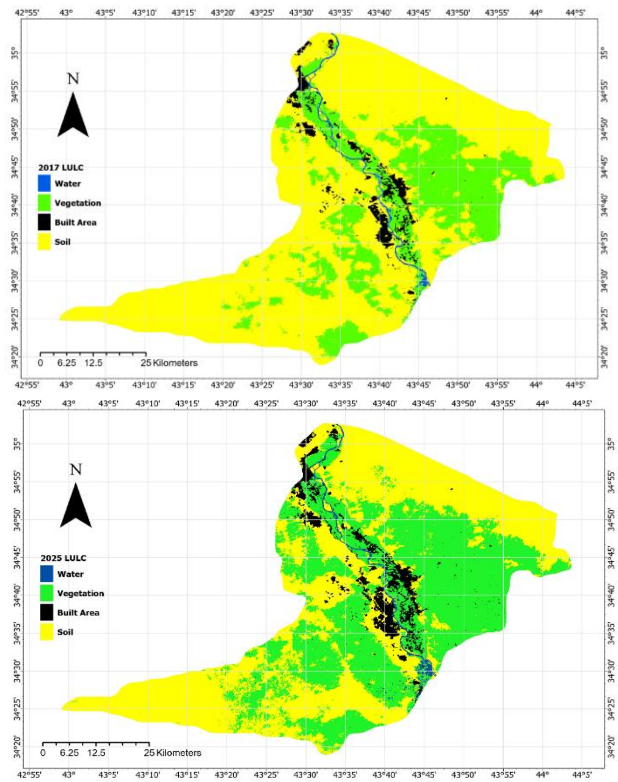

Fig. 2 Land Use/Land Cover (LULC) maps of Tikrit City for 2017 and 2025

The total classified area was approximately 329,512.80 ha (Table 2). In 2017, the dominant LULC class was soil, covering 232,380.28 ha (70.52% of the study area). The class diminished significantly to 164,376.42 ha in 2025, which represents 49.88% of the total area. This means a net decrease of 68,003.86 ha, or a relative decrease of 29.26%.

Table 2. LULC area statistics during 2017-2025

LULC class	Area 2017 (ha)	Area 2025 (ha)	Change (ha)	2017 (%)	2025 (%)	Relative change (%)
Water	2,991.45	3,603.35	+611.89	0.91	1.09	+20.45
Vegetation	83,998.93	145,378.05	+61,379.11	25.49	44.12	+73.07
Built Area	10,142.13	16,154.98	+6,012.85	3.08	4.90	+59.29
Soil	232,380.28	164,376.42	-68,003.86	70.52	49.88	-29.26
Total	329,512.80	329,512.80	—	100.00	100.00	—

In contrast, Vegetation increased substantially during the study period. Its area increased from 83,998.93 ha in 2017 to 145,378.05 ha in 2025, as listed in Table 2. This represents an increase from 25.49% to 44.12% of the total area, with a net gain of 61,379.11 ha and a relative increase of 73.07%. Built Area also increased from 10,142.13 ha to 16,154.98 ha, while Water showed a slight increase from 2,991.45 ha to 3,603.35 ha. These changes are visually supported by the spatial distribution of LULC classes shown in Figure 2.

To further illustrate the relative change in each LULC class, the percentage distribution of the four classes for 2017 and 2025 is shown in Figure 3. The figure confirms the marked reduction in Soil and the corresponding increase in Vegetation during the study period. To evaluate the reliability of the LULC classification before interpreting the spatial changes, an accuracy assessment was performed for the 2017 and 2025 classified maps. The confusion matrices and accuracy indicators are presented in Table 3.

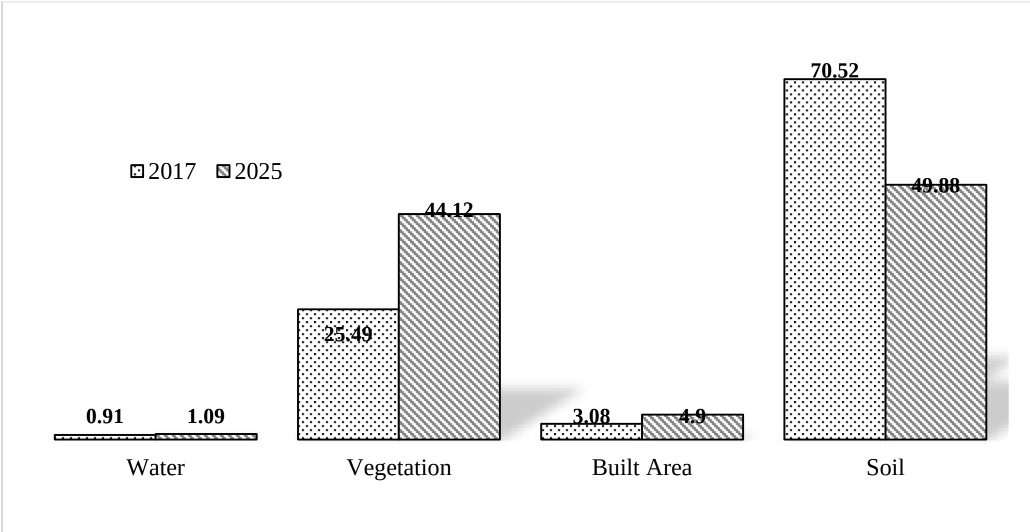

Fig. 3 Percentage distribution of LULC classes in Tikrit City for 2017 and 2025

Table 3. Confusion matrix and accuracy assessment of the LULC classification for 2017 and 2025

Classified \ Reference	Water	Vegetation	Built Area	Soil	Row Total	User's Accuracy (%)
2017 LULC classification						
Water	45	2	1	2	50	90
Vegetation	3	41	3	3	50	82
Built Area	2	4	40	4	50	80
Soil	2	4	5	39	50	78
Column Total	52	51	49	48	200	
Producer's Accuracy (%)	86.54	80.39	81.63	81.25		
2025 LULC classification						
Water	45	2	2	1	50	90
Vegetation	3	42	4	1	50	84
Built Area	2	3	41	4	50	82
Soil	2	3	3	42	50	84
Column Total	52	50	50	48	200	
Producer's Accuracy (%)	86.54	84	82	87.5		

The findings of the accuracy assessment state that the classification results from both years of study were acceptable. The LULC classification of the year 2017 has shown an overall accuracy value of 82.50 and a Kappa coefficient of 0.767. In comparison, the classification performed in the year 2025 has obtained an overall accuracy value of 85.00 and a Kappa coefficient of 0.800. Both of these results show a good level of agreement between the produced classifications and the interpreted reference data. The producers' and users' accuracy measures also proved to be acceptable for most of the classes, with certain groups of Vegetation, Built Area, and Soil confused. This mix-up is expected given the heterogeneous urban and peri-urban nature of the areas studied, which likely include mixed cover conditions represented by Landsat pixels. The LULC transition matrix in Table 4 provides a more detailed interpretation of the direction and magnitude of land-cover conversion between 2017 and 2025. The values in Table 4 represent transition areas in hectares, while the values in parentheses represent the percentage of each 2017 class that changed into each 2025 class.

Table 4. LULC transition matrix during 2017-2025

2017 class / 2025 class	Water	Vegetation	Built Area	Soil	total
Water	2,497.17 (83.5%)	271.08 (9.1%)	39.88 (1.3%)	183.32 (6.1%)	2,991.45
Vegetation	576.79 (0.7%)	78,936.18 (94.0%)	2,009.12 (2.4%)	2,476.84 (2.9%)	83,998.93
Built Area	7.72 (0.1%)	156.12 (1.5%)	9,687.09 (95.5%)	291.20 (2.9%)	10,142.13
Soil	521.66 (0.2%)	66,014.66 (28.4%)	4,418.90 (1.9%)	161,425.06 (69.5%)	232,380.28
Total	**3,603.35**	**145,378.05**	**16,154.98**	**164,376.42**	**329,512.80**
Values represent the transition area in hectares; values in parentheses represent row percentage relative to each 2017 class.					

The largest transition was from Soil to Vegetation, covering 66,014.66 ha, which represents 28.4% of the 2017 Soil class. This transition explains the substantial increase in Vegetation observed in Table 2 and Figure 2. The transition matrix also shows that 161,425.06 ha of Soil remained unchanged, representing 69.5% of the 2017 Soil class, as shown in Table 4.

Built Area showed high persistence, where 9,687.09 ha, equivalent to 95.5% of the 2017 Built Area class, remained built-up in 2025. Similarly, Vegetation showed strong stability, with 78,936.18 ha, or 94.0%, remaining as Vegetation. In addition, 4,418.90 ha of Soil changed into Built Area, indicating moderate urban expansion during the study period. These dominant transition pathways are visually summarized in Figure 4, which illustrates the main direction of land-cover conversion between 2017 and 2025.

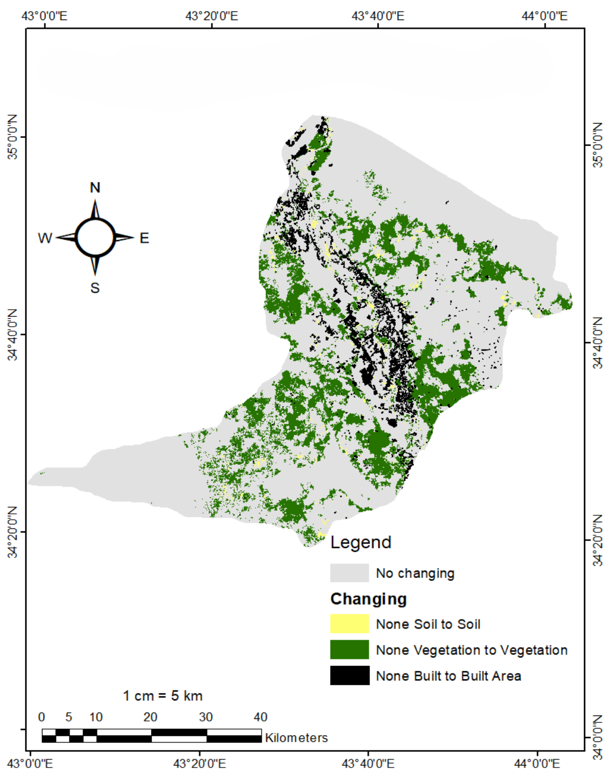

Fig. 4 LULC transition pattern in Tikrit City during 2017–2025

4.2. NDVI Spatial and Statistical Variation

Normalized Difference Vegetation Index (NDVI) maps for the years 2017 and 2025 are presented in Figure 5. These NDVI maps were measured in order to determine the spatial variation in vegetation across Tikrit City and substantiate the interpretation of LULC changes presented in Section 4.1.

Additionally, since both years' images were acquired in March, the NDVI comparison was done in relatively similar weather conditions, thus managing to limit the effect of differences in vegetation in different seasons.

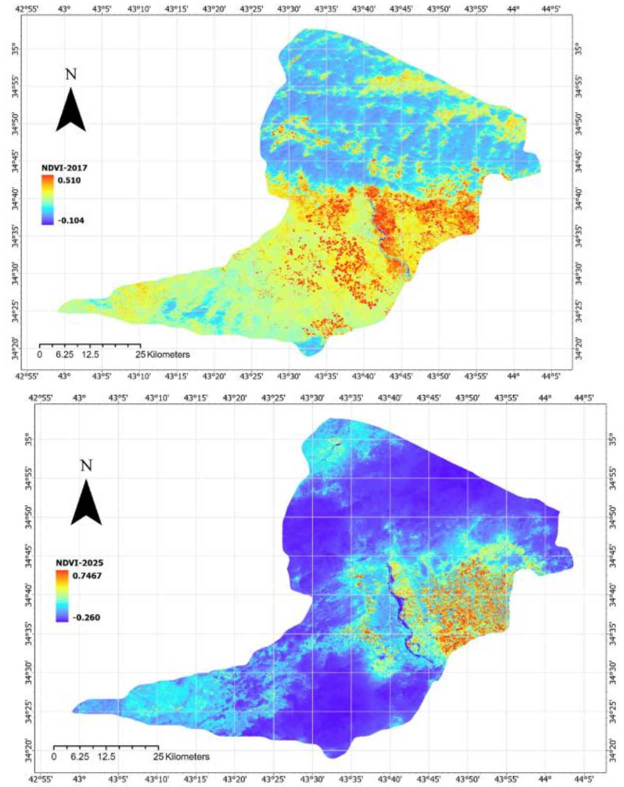

Fig. 5 Normalized Difference Vegetation Index (NDVI) maps of Tikrit City for 2017 and 2025

According to the data in Table 5, the mean NDVI increased from 0.061 in 2017 to 0.075 in 2025. This result is consistent with the LULC results in Table 2, where the Vegetation class increased from 25.49% to 44.12% of the study area. The maximum NDVI also increased from 0.449 in 2017 to 0.532 in 2025, indicating that some locations showed a stronger vegetation response in 2025.

Table 5. Descriptive statistics of NDVI for 2017 and 2025

Statistic	NDVI 2017	NDVI 2025
Number of observations	4124	4124
Minimum	-0.029	-0.160
Maximum	0.449	0.532
Range	0.478	0.693
1st quartile	0.008	-0.005
Median	0.062	0.036
3rd quartile	0.092	0.119
Mean	0.061	0.075
Standard deviation	0.059	0.111
Skewness	1.226	1.748
Kurtosis	3.295	3.078

Although the mean NDVI increased in 2025, the median decreased from 0.062 to 0.036, and the standard deviation increased from 0.059 to 0.111. This indicates that the NDVI change was spatially heterogeneous rather than uniform across the study area. In other words, some locations showed stronger vegetation response in 2025, while other locations remained weakly vegetated or non-vegetated.

To statistically evaluate the temporal change in NDVI, a paired comparison was performed using the same 4124 spatial sample points for both years. The paired design is important because each 2017 value was compared with the corresponding 2025 value at the same location.

Table 6. Paired and non-parametric comparison of NDVI between 2017 and 2025

Test	Comparison	Test statistic	p-value	Interpretation
Paired t-test	NDVI 2017 vs NDVI 2025	t = -8.472	<0.0001	Significant increase in mean NDVI
Sign test	NDVI 2025 − NDVI 2017	N^{+} = 2044	0.586	Direction of change not uniform
Wilcoxon signed-rank test	NDVI 2025 − NDVI 2017	V = 4,449,185; z = 2.567	0.010	Significant ranked difference

The paired t-test showed a statistically significant increase in NDVI between 2017 and 2025. Because the difference was calculated as NDVI 2017 minus NDVI 2025, the mean difference was −0.014, with a 95% confidence interval from −0.018 to −0.011. Therefore, the negative sign indicates that NDVI was higher in 2025. However, the effect size was small, with Cohen's d_z of approximately 0.13, indicating that the increase was statistically significant but limited in magnitude.

The Wilcoxon signed-rank test also confirmed a significant ranked difference between the two years. However, the sign test was not significant (p = 0.586), indicating that the direction of NDVI change was not uniform across all sampled locations. This means that the increase in mean NDVI was driven by stronger positive changes in some locations rather than a consistent increase across the entire study area.

Overall, the NDVI results suggest a measurable but spatially uneven increase in vegetation response between 2017 and 2025. This interpretation is consistent with the LULC transition results, especially the conversion of a considerable part of Soil into Vegetation, while also acknowledging that some areas remained weakly vegetated or showed lower NDVI values.

4.3. LST Spatial Distribution and Temporal Variation

The maps shown in Figure 6 represent Land Surface Temperature (LST) maps of the two observed years of 2017 and 2025. The information from this maps was utilized in order to assess the thermal difference of study area and to help understand the correlation between LST and Land Use Land Cover (LULC), and Normalized Difference Vegetation Index (NDVI). As both images were taken in the month of March, seasonal impacts were limited, and consistency of comparison was achieved.

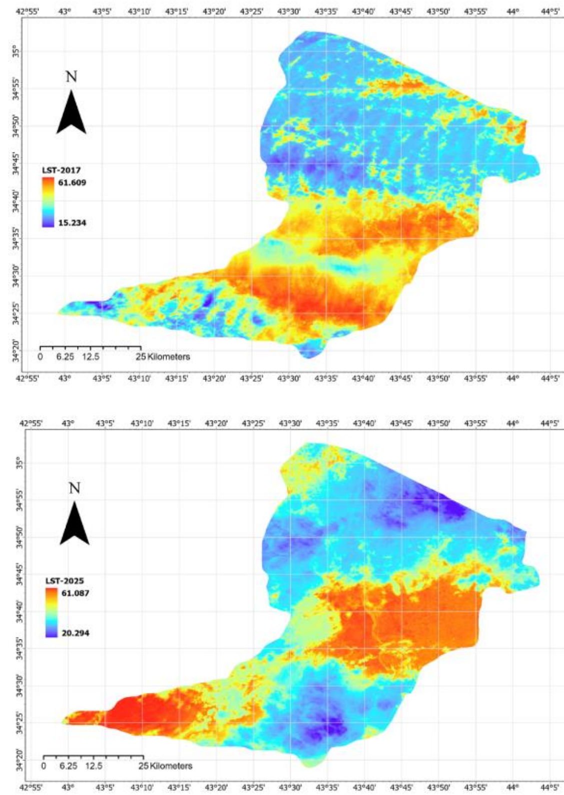

Fig. 6 Land Surface Temperature (LST) maps of Tikrit City for 2017 and 2025

Table 7. Descriptive statistics of LST for 2017 and 2025

Statistic	LST 2017 (°C)	LST 2025 (°C)
Number of observations	4124	4124
Minimum	18.952	20.992
Maximum	60.800	59.559
Range	41.848	38.567
1st quartile	32.748	34.105
Median	40.691	39.146
3rd quartile	50.584	51.405
Mean	41.992	42.031
Standard deviation	9.683	9.628
Skewness	0.273	0.376
Kurtosis	-1.320	-1.229

As shown in Table 7, the mean LST remained almost unchanged between the two years. The mean LST was 41.992°C in 2017 and 42.031°C in 2025, indicating a very small increase of only 0.039°C. However, the spatial distribution of LST values changed between the two years, as reflected by changes in the minimum, maximum, median, quartiles, and non-parametric test results. The analysis was based on 4124 paired spatial sample points extracted from identical locations in both years.

Although the mean LST remained nearly stable, Table 7 shows that the median decreased from 40.691°C in 2017 to 39.146°C in 2025, while the third quartile increased slightly from 50.584°C to 51.405°C. This suggests that the surface temperature distribution was not uniform across the study area. Some locations showed cooling, while others showed higher LST values in 2025. The slightly positive skewness values indicate that LST values were mildly right-skewed in both years, while the negative kurtosis values indicate relatively flat distributions.

To test whether the temporal change in LST was statistically significant, paired and non-parametric tests were applied using the same sample locations for both years. The results are summarized in Table 8.

Table 8. Paired and non-parametric comparison of LST between 2017 and 2025

Test	Comparison	Test statistic	p-value	Interpretation
Paired t-test	LST 2017 vs LST 2025	t = -0.200	0.841	No significant change in mean LST
Sign test	LST 2025 − LST 2017	N^{+} = 2303	<0.0001	Significant directional spatial change
Wilcoxon signed-rank test	LST 2025 − LST 2017	V = 4,482,958; z = 3.009	0.003	Significant ranked distributional change

The results of the paired t-test showed that there was no significant change in LST from 2017 to 2025. The mean difference calculated as LST 2017 minus LST 2025 was −0.039°C, and the 95% confidence interval was found to be from −0.421 to 0.343°C. The significance of the null hypothesis can be ascertained from the fact that the confidence interval includes zero. The effect size in this case is also negligible, and Cohen's dz was calculated to be approximately 0.003, thus indicating that the averaging thermal difference between the years under consideration was just very small.

However, the sign test and the Wilcoxon signed-rank test showed significant differences in the paired LST distribution. The sign test result indicates that the number of locations with increased LST in 2025 was significantly higher than expected by chance. The Wilcoxon signed-rank test also confirmed a significant difference in the ranked paired LST values. Therefore, these non-parametric results indicate a spatial redistribution of LST rather than a meaningful change in the overall mean temperature.

Therefore, the correct interpretation is that the average LST did not change significantly, but the spatial distribution of LST changed significantly between 2017 and 2025. This explains why the LST maps in Figure 6 may show noticeable local thermal differences even though the overall mean LST remained nearly constant.

These findings indicate that the increase in vegetation cover and the reduction in bare soil did not produce a uniform cooling response across the entire study area. Instead, the thermal response varied spatially, which may be related to differences in land-cover composition, vegetation condition, soil exposure, moisture availability, and built-up expansion. This interpretation provides the basis for the following analysis of the relationships among LST, NDVI, and LULC classes.

4.4. Statistical Relationship between NDVI and LST

Before evaluating the statistical relationship between Normalized Difference Vegetation Index (NDVI) and Land Surface Temperature (LST), the normality of NDVI, LST, and their temporal-change variables was examined. The analysis was performed using the paired sample dataset extracted from 4124 identical spatial locations in 2017 and 2025. The results of the Shapiro–Wilk and Anderson–Darling tests are summarized in Table 9.

Table 9. Normality tests for NDVI, LST, and temporal-change variables

Variable	Shapiro–Wilk W	Shapiro–Wilk p-value	Anderson–Darling A^2	Anderson–Darling p-value	Interpretation
NDVI 2025	0.804	<0.0001	238.932	<0.0001	Not normally distributed
NDVI 2017	0.910	<0.0001	60.957	<0.0001	Not normally distributed
LST 2025	0.913	<0.0001	139.546	<0.0001	Not normally distributed
LST 2017	0.919	<0.0001	124.760	<0.0001	Not normally distributed
ΔNDVI	0.936	<0.0001	73.750	<0.0001	Not normally distributed
ΔLST	0.985	<0.0001	22.548	<0.0001	Not normally distributed

As shown in Table 9, all variables significantly departed from normality. This result justified the use of both parametric and non-parametric statistical methods. Therefore, Pearson correlation and linear regression were used to evaluate the linear relationship, while Spearman correlation was used to confirm the monotonic relationship under non-normal data conditions. This dual approach was adopted to avoid relying on a single statistical assumption and to provide a more robust interpretation of the NDVI–LST relationship.

The scatter plots between NDVI and LST for 2017 and 2025 are presented in Figure 7. These plots were used to visualize the direction and strength of the NDVI–LST relationship in both years.

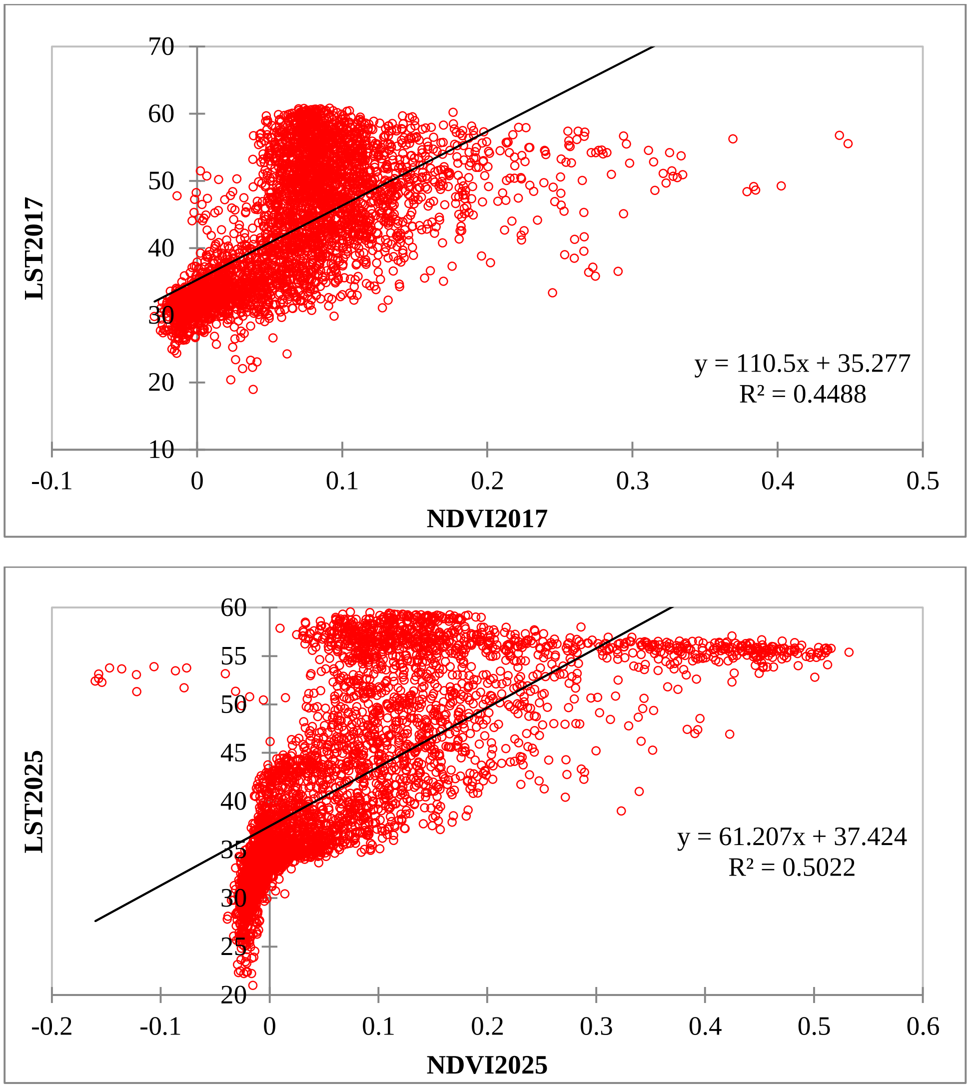

Fig. 7 Scatter plots and regression lines between NDVI and LST for 2017 and 2025

The correlation coefficients in Table 10 also represent effect-size indicators. The Pearson correlation increased from 0.670 in 2017 to 0.709 in 2025, indicating a stronger linear association between NDVI and LST in 2025. Similarly, the Spearman correlation increased from 0.764 to 0.849, confirming that the monotonic relationship also became stronger.

The positive values in Table 10 indicate that locations with higher NDVI values also tended to have higher LST values. This result differs from the commonly expected negative NDVI–LST relationship and should not be interpreted as a simple vegetation-cooling effect. Instead, it suggests that the NDVI–LST relationship in Tikrit City was influenced by land-cover composition, mixed pixels, soil-to-vegetation transitions, agricultural activity, surface moisture variation, and seasonal conditions during March.

Linear regression models were then developed to quantify the relationship between NDVI and LST in each year. The results are shown in Table 11.

Table 10. Pearson and Spearman correlation between NDVI and LST

Case	n	Pearson r	Pearson p-value	Spearman ρ	Spearman p-value	Interpretation
2017: NDVI–LST	4124	0.670	<0.0001	0.764	<0.0001	Strong positive relationship
2025: NDVI–LST	4124	0.709	<0.0001	0.849	<0.0001	Very strong positive relationship
ΔNDVI–ΔLST	4124	0.631	<0.0001	0.744	<0.0001	Strong positive relationship

Table 11. Linear Regression models for NDVI–LST relationships

Case	Regression equation	R²	Adjusted R²	RMSE (°C)	F-value	p-value
2017	$LST_{2017} = 35.277 + 110.495NDVI_{2017}$	0.449	0.449	7.190	3355.847	<0.0001
2025	$LST_{2025} = 37.424 + 61.207NDVI_{2025}$	0.502	0.502	6.794	4158.273	<0.0001
Temporal change	$\Delta LST = -1.003 + 71.900\Delta NDVI$	0.398	0.398	9.712	2727.388	<0.0001

As listed in Table 10, the regression model for 2017 was statistically significant $(F = 3355.847, p < 0.0001)$, with $R^2 = 0.449$. This means that NDVI explained approximately 44.9% of the spatial variation in LST in 2017. In 2025, the model was also highly significant $(F = 4158.273,\ p < 0.0001)$, with $R^2 = 0.502$, indicating that NDVI explained approximately 50.2% of the spatial variation in LST. The reduction in RMSE from 7.190°C in 2017 to 6.794°C in 2025 suggests a slightly stronger model fit in 2025.

To evaluate whether changes in NDVI were associated with changes in LST at the same locations, the temporal differences were calculated as($\Delta NDVI = NDVI_{2025} - NDVI_{2017}$,; $\Delta LST = LST_{2025} - LST_{2017}$).

The scatter plot between $\Delta NDVI$and $\Delta LST$is shown in Figure 8.

As listed in Table 11**,** the regression model for 2017 was statistically significant, with R^2=0.449. This means that NDVI explained approximately 44.9% of the spatial variation in LST in 2017. In 2025, the model was also highly significant, with R^2 = 0.502, indicating that NDVI explained approximately 50.2% of the spatial variation in LST. Because R^2 represents the proportion of explained variance, these values indicate moderate-to-strong effect sizes for the NDVI–LST relationship. The reduction in RMSE from 7.190°C in 2017 to 6.794°C in 2025 suggests a slightly stronger model fit in 2025.

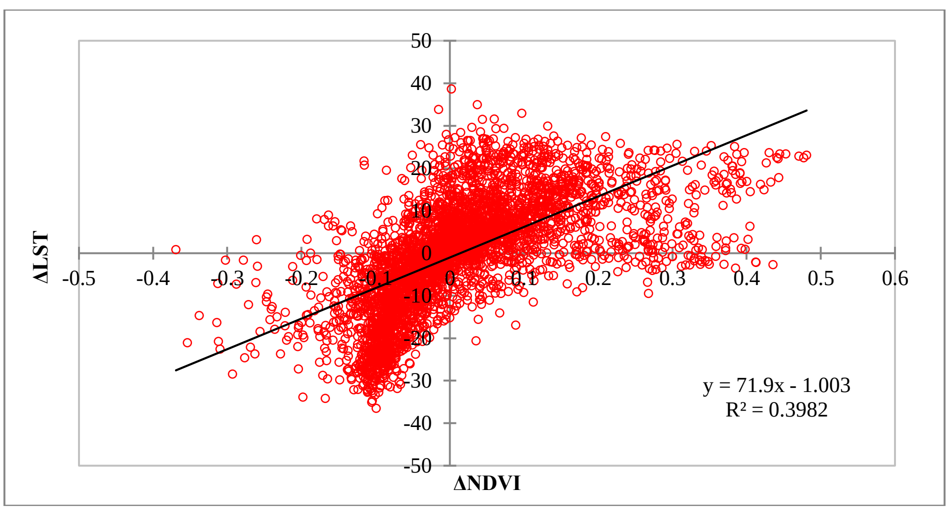

Fig. 8 Relationship between temporal changes in NDVI and LST during 2017–2025

As shown in Table 11 and Figure 8, the regression between $\Delta NDVI$and $\Delta LST$was statistically significant, with $R^2 = 0.398$. This positive slope indicates that locations with greater increases in NDVI also tended to show greater increases in LST. This finding supports the earlier correlation results in Table 10 and confirms that the temporal NDVI–LST relationship in Tikrit City was positive during the March observation period.

Although NDVI increased significantly between 2017 and 2025, as shown previously in Table 6, the overall mean LST did not change significantly, as shown in Table 8. Therefore, the positive $\Delta NDVI–\Delta LST$ relationship does not indicate a simple warming effect caused by vegetation. Rather, it shows that local thermal changes varied spatially and were associated with complex land-cover transitions. In particular, the large conversion from Soil to Vegetation shown in Table 4 may include agricultural or mixed surfaces that exhibit higher NDVI but also higher LST under March surface conditions.

These findings indicate that the NDVI–LST relationship in Tikrit City should be interpreted within the LULC context rather than as a direct vegetation-cooling effect. Therefore, the following section integrates LULC, NDVI, and LST to clarify the land-cover-dependent thermal response.

4.5. Integrated LULC–NDVI–LST Interpretation

To clarify the thermal behavior of Tikrit City, LST values were examined according to the LULC classes for 2017 and 2025. This class-based analysis was used to explain why the NDVI–LST relationship was positive, as shown in Tables 10 and 11, rather than showing a simple vegetation-cooling pattern.

Therefore, examining LST within each LULC class provides a clearer interpretation of how different surface-cover types contributed to the spatial thermal response.

The distribution of LST values for each LULC class is shown in Figure 9. These boxplots illustrate the variability of LST within Water, Vegetation, Built Area, and Soil classes and support the class-based thermal statistics presented in Table 12.

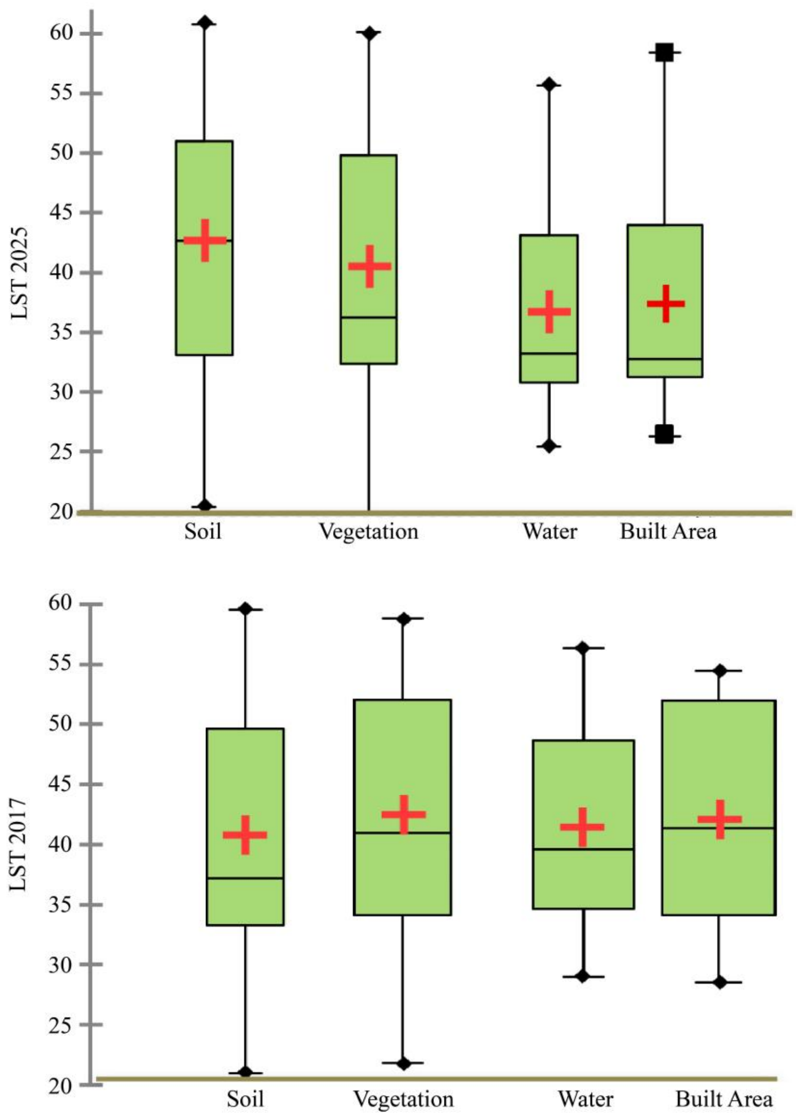

Fig. 9 Boxplots of Land Surface Temperature (LST) by LULC class for 2017 and 2025

According to Table 12, the dominant thermal class has changed from 2017 to 2025. In 2017, the Soil has the greatest mean Land Surface Temperature (LST) value at 42.701°C; Vegetation follows with a mean LST of 40.711°C. On the contrary, the Built Area and Water show lower mean LST values of 37.502°C and 37.661°C, respectively. This means that in 2017, exposed soil surfaces were the leading thermal class bringing heat to the environment. The year 2025 brought a change in the thermal class pattern. Built Area has the highest mean LST value of 44.358°C, followed by Vegetation at 43.165°C. At the same time, the mean LST of Soil decreased to 40.806°C. Hence, this shift indicates that the leading thermal contributing class changed from exposed soil surfaces in 2017 to built-up surfaces in 2025. This correlates with LULC outcomes in Table 2, in which Built Area grew from 3.08% to 4.90%, meanwhile the Soil class decreased from 70.52% to 49.88%.

Table 12. LST statistics by LULC class for 2017 and 2025

Year	LULC class	n	Mean LST (°C)	SD	Min	Max
2017	Water	36	37.661	9.084	25.721	57.666
2017	Vegetation	1028	40.711	9.774	18.952	60.208
2017	Built Area	134	37.502	8.803	26.241	58.938
2017	Soil	2926	42.701	9.585	20.369	60.800
2025	Water	49	42.402	8.020	30.011	57.266
2025	Vegetation	1807	43.165	9.255	22.476	59.476
2025	Built Area	200	44.358	9.391	29.161	58.008
2025	Soil	2068	40.806	9.845	20.992	59.559

In order to confirm whether there were any statistically significant differences between LULC classes, one-way ANOVA was performed separately for 2017 and 2025. However, the criteria for a successful ANOVA test were evaluated prior to interpreting the results. The tests for normality, which are summarized in Table 9, suggested that LST means were not normally distributed, while the information in Table 12 indicates that the group sizes are unequal. Therefore, ANOVA results should be interpreted carefully, and Games-Howell post hoc tests applied, since that statistical method is appropriate under conditions of unequal sample sizes and non-homogeneity of variances. The results are summarized in Table 13.

Table 13. ANOVA results for LST differences among LULC classes

Year	Test	df	F-value	p-value	Interpretation
2017	One-way ANOVA	3, 41	23.608	<0.0001	Significant LST differences among LULC classes
2025	One-way ANOVA	3, 41	23.813	<0.0001	Significant LST differences among LULC classes

As shown in Table 13, LST differed significantly among LULC classes in both years. In 2017, the ANOVA result confirmed that the thermal behavior varied among Water, Vegetation, Built Area, and Soil. In 2025, the ANOVA result was also significant, indicating that LULC classes continued to have a clear influence on the spatial distribution of LST. From the post-hoc comparisons conducted using the Games-Howell test, it had been discovered that the intensity of thermal contrasts was not equal across the two years. In 2017, Soil was found to dominate the thermal classification; this suggests that bare soil surfaces were the major sources of high LST under dry conditions. LST distribution was found to shift from 2017 to 2025, with Built Area having the highest average LST, while Vegetation also recorded significantly elevated temperatures compared to Soil. Such a pattern indicates a transition in thermal pattern towards built-up and mixed or seasonal vegetation areas.

Even though the ANOVA findings were significant from a statistical perspective, it is prudent to be cautious when interpreting the results since not only LULC class determine the variations of LST. There are various other factors, like vegetation density, surface moisture, exposed soil fraction, mixed pixels, and seasonal land-cover conditions, that are associated with LST variations. Thus, class-based analysis is used to corroborate the results rather than serving as evidence that LULC class is the only factor responsible for LST modifications. The integrated reading of Tables 10-13 reveals that NDVI is insufficient to explain the spatial behaviour of LST completely. In fact, even if vegetation is increasing significantly from the year 2017 to the year 2025, the relationship between NDVI and LST remains positive. This indicates that many vegetated pixels may represent land that is a combination of soil and vegetation or may contain seasonal vegetation instead of dense, continuous urban green areas. In March, surface conditions, this area may record higher NDVI while having high surface temperatures as well. The positive relationship between $\Delta NDVI$ and ΔLST, shown previously in Table 11 and Figure 8, further supports this interpretation. Locations with increasing NDVI did not necessarily experience cooling. Instead, the results indicate that surface thermal behavior was controlled by the combined effects of land-cover transition, surface moisture, vegetation density, exposed soil, and urban expansion. From a practical perspective, the increase in Built Area and its highest mean LST in 2025 suggest that future land-management strategies should consider urban expansion as an emerging contributor to local thermal stress in Tikrit City.

5. Conclusion

This study integrated Land Use/Land Cover (LULC), normalized difference vegetation index (NDVI), and Land Surface Temperature (LST) to evaluate surface-cover and thermal changes in Tikrit City, Iraq, between 2017 and 2025. Based on the results, the main conclusions can be summarized as follows:

1. The LULC analysis revealed a clear transformation in surface-cover composition. Soil decreased from 70.52% in 2017 to 49.88% in 2025, while Vegetation increased from 25.49% to 44.12%. Built Area also increased from 3.08% to 4.90%, indicating moderate urban expansion.
2. The transition analysis showed that the dominant land-cover conversion was from Soil to Vegetation, covering 66,014.66 ha. This transition was the main driver of the observed increase in vegetation cover, while the expansion of Built Area indicates an emerging urban influence on the surface-cover structure.
3. NDVI increased significantly between 2017 and 2025, with the mean value rising from 0.061 to 0.075. However, the effect size was small, indicating that the increase was statistically detectable but spatially uneven. This was supported by the non-parametric results, which showed that NDVI change was not uniform across all sampled locations.
4. The mean LST remained statistically stable, increasing only slightly from 41.992°C in 2017 to 42.031°C in 2025. The paired t-test showed no significant change in mean LST, while the non-parametric tests indicated significant spatial redistribution of surface temperature. Therefore, the thermal change was mainly local and spatial rather than a uniform increase in average LST.
5. The NDVI–LST relationship was positive in both years. Pearson correlation increased from r= 0.670 in 2017 to r=0.709 in 2025, while R^2 increased from 0.449 to 0.502. This indicates that NDVI explained a moderate proportion of LST variation, but the positive relationship should not be interpreted as a direct vegetation-cooling effect. Instead, it reflects the combined influence of mixed pixels, agricultural vegetation, exposed soil, surface moisture variation, seasonal conditions, and land-cover composition.
6. The class-based thermal analysis showed that the main heat-contributing class shifted from Soil in 2017 to Built Area in 2025. This finding highlights the practical importance of monitoring built-up expansion, improving the continuity and quality of vegetation cover, and reducing exposed soil surfaces. Future studies should include multi-seasonal images, higher-resolution satellite data, field validation, and hydrological modeling to better quantify the effects of land-cover change on surface moisture, runoff potential, and urban thermal behavior.

These findings confirm the value of integrating LULC, NDVI, and LST for interpreting surface thermal behavior in rapidly changing urban and peri-urban environments.

Ethical Statement

The study made use of available public remote-sensing data; therefore, no humans, animals, identities, or field intervention were involved. Therefore, there was no need for ethical approval. The data were exclusively used for scientific explanation and academic research purposes.

Conflict of Interest

The authors declare that they have no conflict of interest.

Data Availability Statement

The satellite information that was obtained for this study was collected using the open, publicly available Landsat Collection 2 Level-2 satellite data from the USGS EarthExplorer database. The derived data used in this study will be available through the corresponding author, but only upon reasonable request.

References

[1] Bassam F. Al-Bassam, "Land Use/Cover Change Analysis Using Remote Sensing Data: A Case Study, Zhengzhou Area, Henan Province, China," *Al-Khwarizmi Engineering Journal*, vol. 6, no. 2, pp. 72-82, 2010. [Google Scholar] [Publisher Link]

[2] B. V. Ramanamurthy, and B. Vijayasaradhi, "Change Detection Analysis in LULC of the Upstream Thandava Reservoir using RS and GIS Applications," *IOP Conference Series: Materials Science and Engineering*, vol. 1025, 2021. [CrossRef] [Google Scholar] [Publisher Link]

[3] A. Bharath et al., "Assessment of LULC Changes for Hesaraghatta Watershed using GIS Tools and Remote Sensed Data," *Nature Environment and Pollution Technology*, vol. 20, no. 4, pp. 1749-1756, 2021. [CrossRef] [Google Scholar] [Publisher Link]

[4] Zhe Zhu, "Change Detection Using Landsat Time Series: A Review of Frequencies, Preprocessing, Algorithms, and Applications," *ISPRS Journal of Photogrammetry and Remote Sensing*, vol. 130, pp. 370-384, 2017. [CrossRef] [Google Scholar] [Publisher Link]

[5] Ali Kadhim Hussein et al., "Monitoring Land Use and Land Cover Changes Using Remote Sensing and GIS Techniques, A Case Study: Kufa and Najaf, Iraq," *Iraqi Journal of Science*, vol. 66, no. 6, pp. 2603-2614, 2025. [CrossRef] [Google Scholar] [Publisher Link]

[6] Mahmoud Shteiw, F. Zarzoura, and Zaid Jumaah, "A Comparative Study of the Different Remote Sensing Techniques for Evaluating Land Use/Cover in Basra City, Iraq," *Mansoura Engineering Journal*, vol. 45, no. 4, pp. 21-32, 2021. [CrossRef] [Google Scholar] [Publisher Link]

[7] Marwa K. Tawfik, and Alaa M. Al-Lami, "Assessment of the Impact of Climate Change on Land Use/Land Cover for Southern Iraq Using Landsat Data," *IOP Conference Series: Earth and Environmental Science*, vol. 1489, pp. 1-15, 2025. [CrossRef] [Google Scholar] [Publisher Link]

[8] J.W. Rouse et al., "Monitoring Vegetation Systems in the Great Plains with ERTS," *Third Earth Resources Technology Satellite-1 Symposium*, vol. 1, pp. 309-317, 1974. [Google Scholar] [Publisher Link]

[9] Compton J. Tucker, "Red and Photographic Infrared Linear Combinations for Monitoring Vegetation," *Remote Sensing of Environment*, vol. 8, no. 2, pp. 127-150, 1979. [CrossRef] [Google Scholar] [Publisher Link]

[10] Sha Huang et al., "A Commentary Review on the Use of Normalized Difference Vegetation Index (NDVI) in the Era of Popular Remote Sensing," *Journal of Forestry Research*, vol. 32, no. 1, pp. 1-6, 2021. [CrossRef] [Google Scholar] [Publisher Link]

[11] Wissanupong Kliengchuay et al., "Variation of Vegetation Cover and the Relationship with Land Surface Temperature Across Thailand (2007 to 2022)," *Scientific Reports*, vol. 15, pp. 1-17, 2025. [CrossRef] [Google Scholar] [Publisher Link]

[12] Anupam Pandey et al., "Comparing the Seasonal Relationship of Land Surface Temperature with Vegetation Indices and Other Land Surface Indices," *Geology, Ecology, and Landscapes*, vol. 9, no. 4, pp. 1211-1227, 2025. [CrossRef] [Google Scholar] [Publisher Link]

[13] Donglian Sun, and Menas Kafatos, "Note on the NDVI–LST Relationship and the Use of Temperature-Related Drought Indices Over North America," *Geophysical Research Letters*, vol. 34, no. 24, pp. 1-4, 2007. [CrossRef] [Google Scholar] [Publisher Link]

[14] Shipra Singh et al., "Establishing the Relationship Between Land Use Land Cover, Normalized Difference Vegetation Index and Land Surface Temperature: A Case of Lower Son River Basin, India," *Geography and Sustainability*, vol. 5, no. 2, pp. 265-275, 2024. [CrossRef] [Google Scholar] [Publisher Link]

[15] Dino Bečić, and Mateo Gašparović, "Urban Heat Islands and Land-Use Patterns in Zagreb: A Composite Analysis Using Remote Sensing and Spatial Statistics," *Land*, vol. 14, no. 7, pp. 1-26, 2025. [CrossRef] [Google Scholar] [Publisher Link]

[16] Heman Abdulkhaleq A. Gaznayee et al., "Drought Severity and Frequency Analysis Aided by Spectral and Meteorological Indices in the Kurdistan Region of Iraq," *Water*, vol. 14, no. 19, pp. 1-29, 2022. [CrossRef] [Google Scholar] [Publisher Link]

[17] Carol R. Jacobson, "Identification and Quantification of the Hydrological Impacts of Imperviousness in Urban Catchments: A Review," *Journal of Environmental Management*, vol. 92, no. 6, pp. 1438-1448, 2011. [CrossRef] [Google Scholar] [Publisher Link]

[18] Claire J. Oswald et al., "Integrating Urban Water Fluxes and Moving Beyond Impervious Surface Cover: A Review," *Journal of Hydrology*, vol. 618, 2023. [CrossRef] [Google Scholar] [Publisher Link]

[19] Landsat 8–9 Collection 2 Level-2 Science Product Guide. U.S. Department of the Interior, U.S. Geological Survey, 2024. [Online]. Available: https://www.usgs.gov/media/files/landsat-8-9-collection-2-level-2-science-product-guides

[20] Dipesh Oli et al., "Assessment of Land Use Land Cover Change and its Impact on Variations of Land Surface Temperature in Atlanta, USA," *Environmental and Sustainability Indicators*, vol. 26, pp. 1-16, 2025. [CrossRef] [Google Scholar] [Publisher Link]

[21] John A. Richards, and Xiuping Jia, *Remote Sensing Digital Image Analysis: An Introduction*, 4th ed., Springer, 2006. [CrossRef] [Google Scholar] [Publisher Link]

[22] Thomas Lillesand, Ralph W. Kiefer, and Jonathan Chipman, *Remote Sensing and Image Interpretation*, 7th ed., John Wiley & Sons, pp. 1-768, 2015. [Google Scholar] [Publisher Link]

[23] Giles M. Foody, "Status of Land Cover Classification Accuracy Assessment," *Remote Sensing of Environment*, vol. 80, no. 1, pp. 185-201, 2002. [CrossRef] [Google Scholar] [Publisher Link]

[24] Russell G. Congalton, and Kass Green, *Assessing the Accuracy of Remotely Sensed Data: Principles and Practices*, 3rd ed., CRC Press, pp. 1-346, 2019. [CrossRef] [Google Scholar] [Publisher Link]

[25] Ugur Avdan, and Gordana Jovanovska, "Algorithm for Automated Mapping of Land Surface Temperature Using LANDSAT 8 Satellite Data," *Journal of Sensors*, vol. 2016, no. 1, pp. 1-8, 2016. [CrossRef] [Google Scholar] [Publisher Link]